metals

MDPI

Article

Atomistic-Level Insights into MgO and Na_2O Modifications of Molten Aluminosilicate Slag: A Molecular Dynamics Research on Structural Evolution and Properties

Chunhe Jiang [1], Bo Liu [2], Jianliang Zhang [3,*] and Kejiang Li [3,*]

[1] Technical Support Center for Prevention and Control of Disastrous Accidents in Metal Smelting, University of Science and Technology Beijing, Beijing 100083, China; jiangchunhe@ustb.edu.cn
[2] School of Advanced Engineering, University of Science and Technology Beijing, Beijing 100083, China; u202240348@xs.ustb.edu.cn
[3] School of Metallurgical and Ecological Engineering, University of Science and Technology Beijing, Beijing 100083, China
* Correspondence: jl.zhang@ustb.edu.cn (J.Z.); likejiang@ustb.edu.cn (K.L.)

Abstract: Molecular dynamics simulations were employed to systematically investigate the synergistic effects of Na_2O and MgO on the atomistic-scale structural evolution and properties of CaO–SiO_2–Al_2O_3-based slags. By constructing slag models with varying Na_2O/MgO ratios, the variations in pair distribution functions, oxygen structural units, coordination environments, diffusion coefficients, and viscosity were analyzed in detail. Compared with Na_2O, MgO exhibits a stronger ability to disrupt oxygen structural units. The relative content of Na_2O and MgO does not significantly affect the bond lengths within the basic network structure. As the MgO content increases, a greater proportion of bridging oxygens and tricluster oxygens are converted into non-bridging oxygens and free oxygens, markedly reducing the degree of polymerization in the slag network. Although MgO also promotes the formation of tetrahedrally coordinated Al (Al^4) more effectively than Na_2O, its dominant role in enhancing slag fluidity is primarily attributed to its impact on the oxygen structural units. Despite the much higher self-diffusion coefficient of Na^+ compared to Mg^{2+}, MgO more significantly reduces the overall viscosity and enhances the fluidity of the melt than Na_2O. Therefore, although the number of Na atoms is greater under equal mass conditions, Mg demonstrates a considerably stronger capacity to depolymerize the slag structure.

Keywords: MgO/Na_2O; aluminosilicate; molecular dynamics; microstructure; viscosity

check for updates

Received: 13 May 2025
Revised: 7 June 2025
Accepted: 8 June 2025
Published: 12 June 2025

Citation: Jiang, C.; Liu, B.; Zhang, J.; Li, K. Atomistic-Level Insights into MgO and Na_2O Modifications of Molten Aluminosilicate Slag: A Molecular Dynamics Research on Structural Evolution and Properties. *Metals* **2025**, *15*, 656. https://doi.org/10.3390/met15060656

Copyright: © 2025 by the authors. Licensee MDPI, Basel, Switzerland. This article is an open access article distributed under the terms and conditions of the Creative Commons Attribution (CC BY) license (https://creativecommons.org/licenses/by/4.0/).

1. Introduction

In the process of ironmaking and steelmaking, slag not only fulfills traditional roles such as impurity removal, melt protection, and regulation of heat and mass transfer, but also plays a critical role in structural modulation within high-temperature reactive systems [1–3]. Aluminosilicate slags based on the SiO_2-Al_2O_3-CaO system are widely employed in various metallurgy processes, including blast furnaces, electric arc furnaces, and converters. The microscopic structure of these slags directly influences their thermophysical properties [4,5] as well as the thermodynamic and kinetic behavior of metallurgical reactions. In particular, the atomistic-scale structural evolution of slags in the liquid state is a key factor governing their flow behavior and thermal stability [6]. Therefore, gaining an in-depth understanding of the structural formation and modulation mechanisms of aluminosilicate slags at the atomistic level has become a crucial research focus in the field of metallurgy.

The fundamental network structure of aluminosilicate slags consists of interconnected three-dimensional frameworks formed by silicon–oxygen (Si-O) and aluminum–oxygen (Al-O) tetrahedral units linked through bridging oxygen atoms (BO) and tricluster oxygen (TO) [7]. This framework governs the degree of structural polymerization of the slag, which in turn influences its viscosity and thermal stability [8]. To meet specific process requirements, network modifiers are typically introduced to disrupt the framework structure and tailor the degree of structural complexity (DSC) and flow characteristics of the slag [9]. Among these, Na_2O is a commonly used alkali metal oxide additive known for its strong network-breaking ability [10]. The incorporation of Na^+ ions tends to break the BO connections between SiO_4 and AlO_4 tetrahedra, generating non-bridging oxygen (NBO) or free oxygen (FO) species. This process reduces the structural polymerization and viscosity while significantly enhancing diffusion properties and thermal conductivity [11]. Due to their high mobility and charge compensation effect, Na^+ ions can also induce the transformation of AlO_4 tetrahedra into five-coordinated AlO_5 structures, and may even promote the cleavage of BOs, thereby intensifying the network depolymerization process.

However, Na_2O is also regarded as a "detrimental component" in the metallurgical industry, as its accumulation in systems such as blast furnaces can lead to adverse effects, including hearth accretion and accelerated erosion of refractory materials [12,13]. Therefore, an in-depth investigation into the structural modulation behavior of Na_2O across different compositional systems, and its impact on atomistic-scale structure and thermophysical properties, is of great significance for optimizing slag design and enhancing process stability. MgO, a commonly used alkaline earth metal oxide in metallurgical slags, exhibits more complex structural roles [14]. On one hand, the strong ionic bonds formed between Mg^{2+} and O^{2-} can enhance the stability of local coordination environments and suppress excessive network depolymerization; on the other hand, Mg^{2+} may synergistically or competitively modulate the network-breaking effect of Na^+, thereby altering the evolution pathways of network units and the energy barriers for structural reconstruction [15]. Existing experimental and computational studies have demonstrated that the addition of MgO can stabilize $[AlO_4]^-$ and $[SiO_4]^{4-}$ tetrahedral units to a certain extent, regulate the formation of NBOs, and, under specific conditions, reduce slag viscosity [16]. Nonetheless, the potential synergistic or antagonistic interactions between Na_2O and MgO in aluminosilicate slags, particularly their combined influence on network structure, oxygen species, atomic diffusion behavior, and key physicochemical properties such as viscosity, remain insufficiently understood at the atomistic scale.

While conventional experimental methods can provide structural and performance information of slags under macroscopic or static conditions, they are limited in capturing the dynamic migration of ions such as Na^+ and Mg^{2+} in the high-temperature liquid state and their real-time effects on the network framework. Molecular dynamics simulations, as a theoretical tool with atomistic-scale spatial and temporal resolution, offer a unique perspective for elucidating the structural evolution and thermophysical regulation mechanisms of slags [6]. In recent years, MD techniques have been extensively applied to investigate coordination environments, oxygen species, and diffusion behaviors in multicomponent slag systems, leading to significant advances [17]. However, most existing studies have focused on single-component systems or conditions with fixed basicity, and systematic investigations into the synergistic regulation behavior of Na_2O–MgO composite systems under varying basicity or compositional conditions remain scarce.

Compared to previous studies that mainly focused on single-component modification or fixed-basicity conditions, this work provides a novel, systematic investigation into the coupled effects of Na_2O and MgO under variable compositional strategies. By analyzing structural evolution mechanisms at the atomic scale and correlating them with dynamic

and thermophysical behavior, our study fills the current knowledge gap in understanding the synergistic or antagonistic roles of Na^+ and Mg^{2+} ions. This work also provides a reference methodology for future simulation-driven designs of advanced slag systems in complex metallurgical environments.

Accordingly, this research employs classical molecular dynamic simulations to construct a series of representative aluminosilicate slag models containing key components such as Si, Al, Ca, Na, Mg, and O. The aim is to systematically investigate the synergistic modulation mechanisms of Na_2O and MgO on the slag structure and properties under various doping strategies and compositional conditions. A range of analytical techniques, including pair distribution functions (PDFs), coordination number (CN) analysis, oxygen species classification, self-diffusion coefficients, and bond angle distributions, are employed to examine the structural construction and depolymerization of the network. This approach enables a comprehensive understanding of how Na^+ and Mg^{2+} regulate the slag network structure and clarifies the coupling mechanism between atomic mobility and macroscopic flow behavior.

2. Simulation Approach

Five sets of experiments were designed, with their detailed compositions presented in Table 1. The effects of Na_2O and MgO on aluminosilicate slag at high temperatures were investigated by varying their relative mass fractions in the system. Molar masses and densities of the constituent atoms were used to calculate the dimensions of the cubic simulation cell. Each experimental configuration contained approximately 10,000 atoms, which were initially distributed randomly within the cell. Periodic boundary conditions were applied throughout to maintain simulation fidelity.

Table 1. The composition and melting point of different simulation models, wt%.

	SiO_2	CaO	MgO	Al_2O_3	Na_2O	Total	Melting Point (K)
N-1	31.82	38.18	1.00	20.00	9.00	100	1597.8
N-2	31.82	38.18	3.00	20.00	7.00	100	1613.5
N-3	31.82	38.18	5.00	20.00	5.00	100	1655.6
N-4	31.82	38.18	7.00	20.00	3.00	100	1688.3
N-5	31.82	38.18	9.00	20.00	1.00	100	1733.6

All molecular dynamics simulations were performed using the LAMMPS package (version 8 February 2023) [18] with a timestep of 1 fs. Initially, a randomized atomic configuration was equilibrated for 100 ps at 5000 K under an NVT ensemble with a Nosé–Hoover thermostat [19]. The system was then quenched to 1873 K at a rate of 1×10^{13} K/s, followed by a 500 ps equilibration during which iterative loops were applied to ensure that the potential energy had fully stabilized. Finally, a 1000 ps production run at 1873 K was conducted to collect trajectory data, which were analyzed using the ISAACS package v2.10 [20] and custom in-house scripts to extract pair distribution functions, coordination numbers, bond-angle distributions, and structural unit statistics.

Molecular dynamics provides a powerful framework for probing materials at the atomistic scale, but its predictive accuracy hinges critically on the choice of interatomic potential. In this research, all atomic interactions were described by the Miyake potential [21], which can be expressed as follows:

$$U(r_{ij}) = \frac{z_i z_j e^2}{r_{ij}} + f_0(b_i + b_j)\exp\left(\frac{a_i + a_j - r_{ij}}{b_i + b_j}\right) - \frac{c_i c_j}{r_{ij}^6} + D_{ij}\left\{\left[1 - e^{-a_{ij}\cdot(r - r_0)}\right]^2\right\} \quad (1)$$

where r_{ij} denotes the distance between atoms i and j, and f_0 (6.9511 × 10^{-11} N) is a scaling constant. The parameters z, a, b, and c characterize the long-range Coulombic interaction, while D_{ij}, a_{ij}, and r_0 specify the cation–anion pair for the short-range Morse potential. The first term thus accounts for Coulombic forces, the second term represents the repulsive Born interaction, the third term captures the attractive van der Waals contribution, and the fourth term embodies the short-range Morse bonding. All numerical values for these parameters are listed in Table 2.

Table 2. The BMH potential parameters developed by Miyake were used in this simulation.

Ion	z (e)	a (Å)	b (Å)	c (Å^3(KJ/mol)$^{1/2}$)	Ion Pair	D (KJ/mol)	a (1/Å)	r_0 (Å)
Si	1.92	0.5983	0.025	0.00	Si-O	63	2	1.47
Ca	0.96	1.1425	0.042	30.74	Al-O	50.4	2	1.58
Mg	0.96	0.9400	0.040	20.49	Ca-O	21	2	2.20
Al	1.44	0.6758	0.030	0.00	Mg-O	42	2	1.75
Na	0.48	1.0450	0.050	20.49	Na-O	-	-	-
O	−0.96	1.7700	0.138	51.23				

In addition to molecular dynamics simulations, thermodynamic calculations were performed using FactSage 7.3 to provide a complementary analysis of viscosity behavior. FactSage is a widely used thermochemical software based on a large body of experimentally measured data. Its viscosity module incorporates a broad range of empirical results, allowing for the reliable prediction of the viscosity of high-temperature systems such as blast furnace slag, coal ash, and coke ash. In this work, the viscosity of oxide melts was predicted using the viscosity module of FactSage 7.3 [22–24]. The FactPS and FToxid databases were selected for the calculations, which enabled us to evaluate the viscosity trends as a function of oxide composition. These thermodynamic predictions serve as a useful benchmark for validating the trends observed in the molecular dynamics simulations.

3. Results and Discussion

3.1. Local Structural Characteristics

The pair distribution function can be employed to reveal the short-range order within melts, thereby establishing a correlation between atomic structure and macroscopic properties. It characterizes the local atomic arrangement within a spherical shell surrounding a given atom and is proportional to the probability of finding another atom within a differential volume element Δr at a distance r. The mathematical expression of the PDF is given as follows:

$$g_{ij}(r) = \frac{V}{N_i N_j} \sum_j \frac{\langle n_{ij}(r - \triangle r/2, r + \triangle r/2) \rangle}{4\pi r^2 \triangle r} \quad (2)$$

Here, $N_i(N_j)$ denotes the total number of atoms of type $i(j)$ in the system under investigation; V represents the total volume of the system; n_{ij} ($r - \Delta r/2$, $r + \Delta r/2$) is the number of j-type atoms located within the spherical shell of thickness Δr centered at a distance r from an i-type atom. The pair distribution function not only characterizes the short-range and long-range order in melts but also provides valuable structural information such as bond lengths and coordination numbers.

By integrating the pair distribution function, the average coordination number of a given atom within a specified radial distance can be obtained. The coordination number is calculated using the following equation:

$$N_{ij}(r) = \frac{4\pi N_j}{V} \int_0^r r^2 g_{ij}(r) dr \quad (3)$$

The pair distribution functions between cations and oxygen atoms in the present system are shown in Figure 1. The position of the first peak in the PDF corresponds to the bond length between two atoms. As observed from Figure 1, the bond lengths in the current system follow the order: Si-O < Al-O < Mg-O < Na-O < Ca-O < O-O. In terms of peak intensity, the Si–O and Al–O bonds exhibit relatively higher peaks, indicating a stronger bond. This observation supports the presence of SiO_4 and AlO_4 tetrahedral units as the primary structural units in aluminosilicate melts.

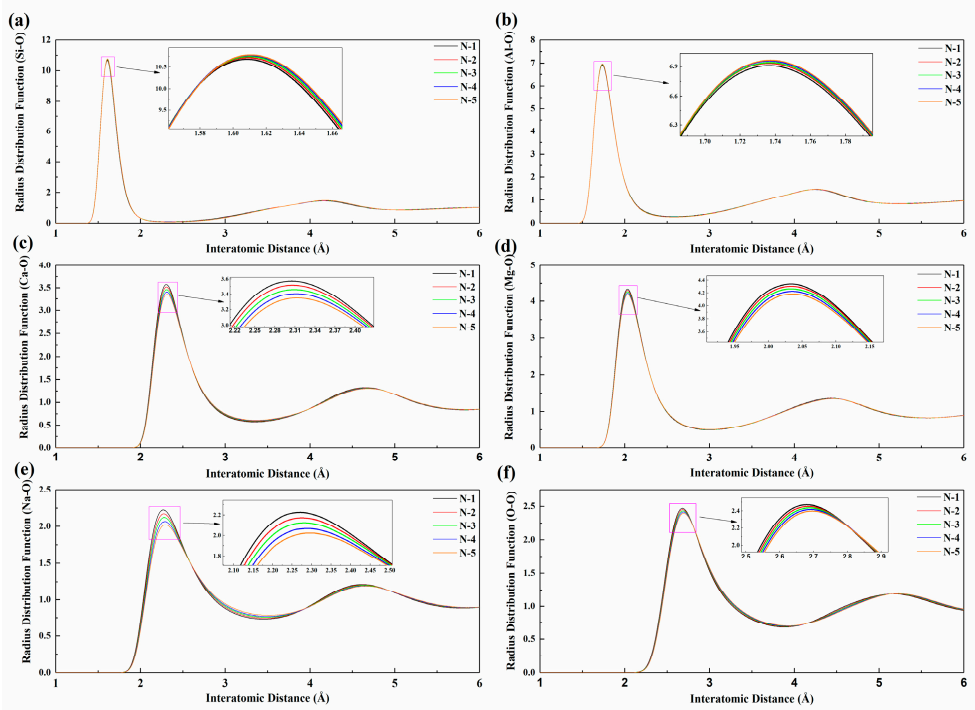


Figure 1. The pair distribution function of different pairs. (**a**) Si-O. (**b**) Al-O. (**c**) Ca-O. (**d**) Mg-O. (**e**) Na-O. (**f**) O-O.

Furthermore, during the variation in the relative content of MgO and Na_2O, a slight decrease in peak intensity of the Si-O and Al-O bonds is observed with decreasing Na_2O content, suggesting a minor weakening of these bonds. Cations such as Ca^{2+}, Mg^{2+}, and Na^+ generally do not form covalent bonds with oxygen atoms in the melt, resulting in comparatively weaker chemical interactions. However, an increase in Na_2O content leads to a slight enhancement in the intensity of these weaker ionic interactions.

To better compare the evolution of chemical bonding, the nearest-neighbor bond lengths, second-nearest-neighbor bond lengths, and coordination numbers were statistically analyzed, as shown in Table 3. It is observed that the bond lengths of Si-O and Al-O are 1.61 Å and 1.73 Å, respectively, and remain unchanged with variations in the relative contents of Na_2O and MgO. The second-nearest-neighbor distances for Si-O and Al-O fall within the ranges of 4.16–4.18 Å and 4.23-4.27 Å, respectively. An increase in the Na_2O content results in a slight reduction in the second-nearest-neighbor distances for both.

Regarding coordination numbers, Si-O pairs exhibit values between 4.04 and 4.07, which are closest to the ideal tetrahedral coordination, confirming the structural stability of SiO_4 tetrahedra in the molten slag. A higher Na_2O content slightly reduces the Si-O coordination number, which in turn promotes the stability of the SiO_4 tetrahedra. For Al-O, the coordination number ranges from 4.32 to 4.45, indicating the coexistence of multiple coordination states, which will be analyzed in more detail later. Notably, an increase in Na_2O content leads to a higher coordination number for Al-O, suggesting that Na_2O facilitates the transformation of Al-O units toward higher coordination states.

In terms of ionic bonds, variations in the relative contents of Na_2O and MgO do not significantly affect the Ca-O and Mg-O bond lengths. However, a decrease in Na_2O content results in a noticeable increase in the Na-O bond length. The second-nearest-neighbor distances, in contrast, exhibit minimal sensitivity to changes in Na_2O and MgO content.

Table 3. The first peak (R_1), the second peak (R_2), and the coordination number (CN) of various ion oxygen pairs.

	Si-O			Al-O			Ca-O			Mg-O			Na-O		
	R1	**R2**	**CN**	**R1**	**R2**	**CN**	**R1**	**R2**	**CN**	**R1**	**R2**	**CN**	**R1**	**R2**	**CN**
N-1	1.61	4.16	4.07	1.73	4.23	4.45	2.31	4.66	7.59	2.03	4.46	5.94	2.27	4.62	7.49
N-2	1.61	4.17	4.06	1.73	4.24	4.42	2.31	4.67	7.57	2.03	4.46	5.89	2.27	4.59	7.50
N-3	1.61	4.17	4.05	1.73	4.26	4.39	2.31	4.68	7.46	2.03	4.44	5.81	2.28	4.63	7.27
N-4	1.61	4.18	4.04	1.73	4.26	4.36	2.31	4.68	7.44	2.03	4.46	5.80	2.29	4.61	7.22
N-5	1.61	4.18	4.04	1.73	4.27	4.32	2.31	4.69	7.42	2.03	4.46	5.72	2.31	4.63	7.26

3.2. The Structural Unit Variation

Previous studies [25] have demonstrated that aluminosilicate-based slags are primarily composed of SiO_4 and AlO_4 tetrahedral units, with oxygen atoms playing a crucial role in linking these structural units, as illustrated in Figure 2. Within the network structure formed by aluminosilicate components, oxygen atoms can be classified into four types: free oxygen, non-bridging oxygen, bridging oxygen, and tricluster oxygen. Free oxygen refers to oxygen atoms that exist independently within the melt without forming chemical bonds with any cation. Non-bridging oxygen is bonded to only one tetrahedron and is typically located at the periphery of the tetrahedral unit. Bridging oxygen atoms are shared by two tetrahedra and serve as linkages between them; a higher BO content indicates a more interconnected and complex network structure. Tricluster oxygen atoms are shared among three tetrahedra and contribute more significantly to the network connectivity than bridging oxygen, reflecting a higher degree of polymerization within the melt structure.

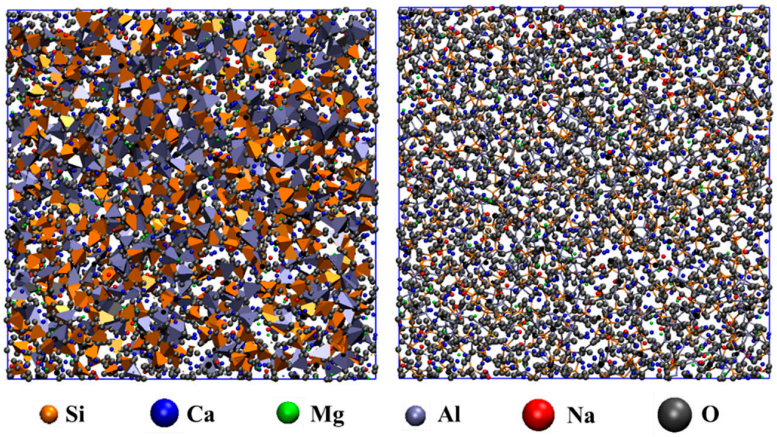


Figure 2. Basic microstructural distribution of aluminosilicate melts.

Figure 3a presents the compositional evolution of the four types of oxygen atoms. It can be observed that as the relative content of Na_2O decreases during variations in Na_2O and MgO concentrations, both BO and TO tend to convert into NBO and FO. Among these, the most significant change occurs between BO and NBO, indicating extensive disruption of the linkages between tetrahedral units. Comparing the effects of Na_2O and MgO, it is evident that MgO exhibits a stronger depolymerizing effect on the network structure than Na_2O. Although the number of Na atoms is considerably higher than that of Mg at equivalent molar ratios, the ability of Na_2O to disrupt the network is relatively weaker.

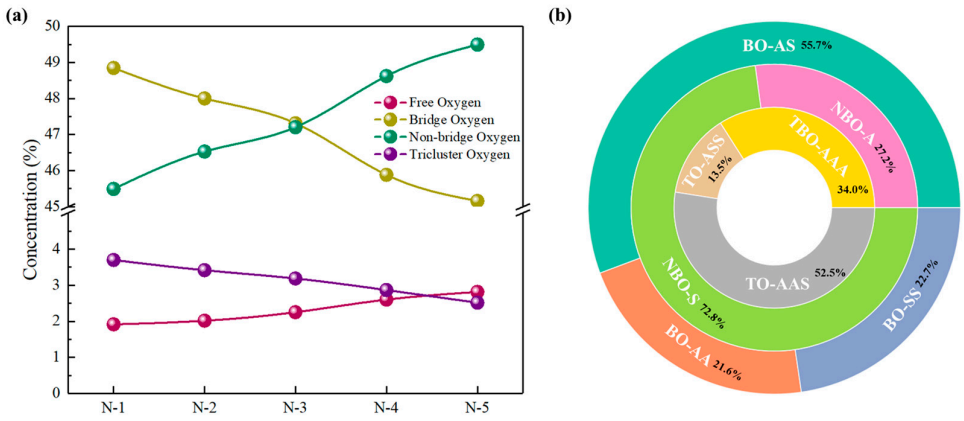


Figure 3. The concentration of oxygen clusters. (**a**) The evolution of bridge oxygen, non-bridge oxygen, free oxygen, and tricluster oxygen. (**b**) The concentration of specific oxygen clusters.

Figure 3b shows the distribution of specific types of oxygen atoms. Changes in the relative content of Na_2O and MgO do not directly alter the proportions of these specific oxygen types. Within the bridging oxygen category, three subtypes are identified: BO-AS (bridging oxygen connecting AlO_4 and SiO_4 tetrahedra), BO-AA (bridging oxygen connecting AlO_4 tetrahedra), and BO-SS (bridging oxygen connecting SiO_4 tetrahedra), accounting for 55.7%, 22.7%, and 21.6% of the total BO, respectively. This indicates that oxygen atoms bridging AlO_4 and SiO_4 tetrahedra are the most abundant. For non-bridging oxygen, only two types are observed: NBO-A and NBO-S. Due to the relatively high content of SiO_2 in the system, NBO-S accounts for as much as 72.8%. Tricluster oxygen atoms are classified into three types—TO-AAS, TO-AAA, and TO-ASS—representing 52.5%, 34.0%, and 13.5% of the total TO, respectively. Given the lower structural stability of AlO_4 tetrahedra compared to SiO_4, all TO types involve participation of AlO_4 units.

Given that the average coordination number of Al-O ranges between 4.32 and 4.45, the evolution of Al-O coordination environments is illustrated in Figure 4. It can be observed that with decreasing Na_2O content, the proportion of Al-4 species gradually increases, indicating a transformation from Al-5 to Al-4 coordination. Under conditions where the relative contents of Na_2O and MgO are equivalent, Na_2O is found to suppress the formation of Al-4 coordinated structures, instead promoting the formation of the less stable Al-5 coordination. However, since the overall network structure exerts a more significant influence on the degree of polymerization within the system, the effect of variations in Al-O coordination environments is less pronounced compared to changes in oxygen structural units.

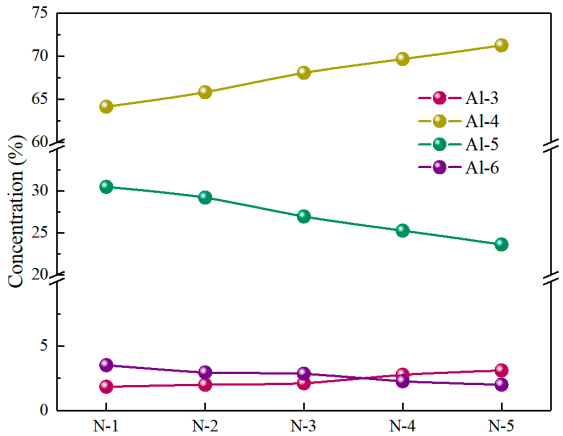


Figure 4. The evolution of different Al units.

3.3. The Distribution of Bond Angle

Aluminosilicate-based slags primarily consist of an interconnected network of SiO_4 and AlO_4 tetrahedra, a structure that directly correlates with the previously discussed variations in oxygen structural units. Therefore, the major bond angles that constitute this network were statistically analyzed, as shown in Figure 5. It is first observed that the Al-O-Al bond angle exhibits a wide fluctuation range, spanning from 80° to 160°, which is directly associated with the existence of multiple coordination states for Al-O. A concentrated distribution is found within the 90–140° range, with a peak near 120°, indicating a significant deviation from the ideal tetrahedral geometry.

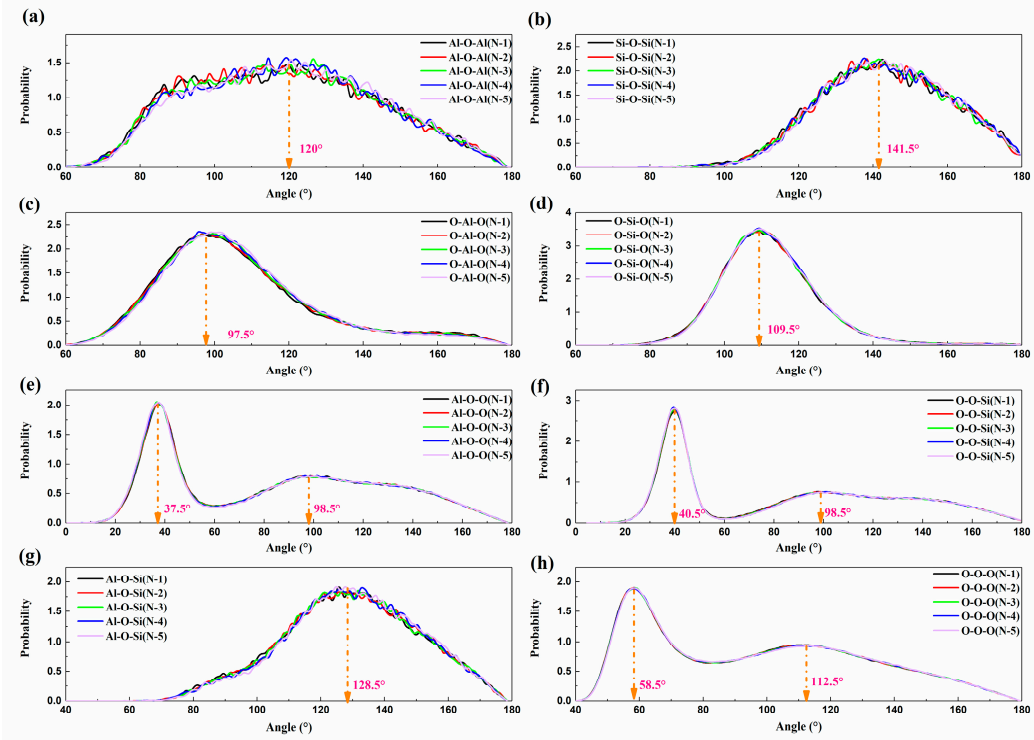


Figure 5. The distribution of bond angles. (**a**) Al-O-Al. (**b**) Si-O-Si. (**c**) O-Al-O. (**d**) O-Si-O. (**e**) Al-O-O. (**f**) O-O-Si. (**g**) Al-O-Si. (**h**) O-O-O.

In contrast, the Si-O-Si bond angle displays a single peak at approximately 141.5°, closely aligning with the standard tetrahedral angle, which further confirms the structural stability of the SiO_4 tetrahedra. The O-Al-O and O-Si-O bond angles are observed at 97.5° and 109.5°, respectively. Given that the ideal bond angle in a regular tetrahedron is 109.5°, this demonstrates that the AlO_4 tetrahedra are less stable than their SiO_4 counterparts. Both Al-O-O and Si-O-O angles show two peaks: the sharper peak corresponds to intra-tetrahedral angles, while the broader one is attributed to the presence of bridging or tricluster oxygen atoms. A similar trend is observed in the O-O-O bond angle distribution. The bond angle between AlO_4 and SiO_4 tetrahedra connected via a bridging oxygen is approximately 128.5°, reflecting the structural arrangement induced by such oxygen species.

3.4. Transport Properties

In contrast to solids, liquid molecular constituents exhibit continuous translational motion rather than maintaining fixed spatial positions. This dynamic behavior enables quantitative characterization through mean square displacement (MSD) analysis [26], which measures the temporal evolution of atomic trajectories. The MSD quantifies the average

spatial deviation of particles over a specified time interval T, calculated through ensemble averaging across multiple temporal origins:

$$MSD = \left\langle \mid r(T) - r(0) \mid^2 \right\rangle = \frac{1}{NM} \sum_{1}^{N} \sum_{k}^{M} \mid r_i(t_k + T) - r_i(t_k) \mid^2 \quad (4)$$

where M denotes the number of time origins, t_k represents the initial time of the k_{th} temporal subset, and $r_i(t_k + T) - r_i(t_k)$ corresponds to the displacement vector of atom i between times t_k and $t_k + T$. Through application of the Einstein relation, these displacement metrics enable determination of self-diffusion coefficients for distinct atomic species using the proportionality $D_i = \mathrm{MSD}/(6\mathrm{T})$.

The macroscopic transport properties of the system can be described by a composite diffusion coefficient derived from individual species contributions [27]:

$$D_{\mathrm{Total}} = \sum_{i=1}^{i=n} D_i \cdot x_i \quad (5)$$

where D_i and x_i respectively represent the self-diffusion coefficient and the mole fraction of atom species i, with n being the total number of atoms in the system.

Figure 6 illustrates the variation in self-diffusion coefficients of different atoms as a function of the relative content of Na_2O and MgO. It is clear that Na^+ ions exhibit the highest diffusion capability, while Mg^{2+} ions show significantly lower diffusion ability compared to Na^+ ions. A decrease in Na_2O content leads to a marked increase in the self-diffusion coefficient of Na^+ ions. However, the effects of changes in Na_2O and MgO content on the diffusion coefficients of other atoms are not consistent. To provide a clearer understanding of the overall impact on atomic diffusion coefficients, the total diffusion coefficient of the system was calculated based on content variations. This allows for a more comprehensive analysis of the slag's flow properties. It is observed that, with the reduction in Na_2O content, the total diffusion coefficient of the system increases significantly, indicating a change in its flowability. Furthermore, the variation in self-diffusion coefficients and flowability is directly related to the complexity of the system's structure. When comparing the relative content changes of Na_2O and MgO, it becomes evident that MgO has a greater ability to enhance the system's flowability than Na_2O. This observation aligns with its influence on the microstructural units and network complexity within the system. Additionally, the viscosity of the system, calculated using both FactSage and molecular dynamics methods, was compared, revealing a decreasing trend in viscosity that further supports the improved flowability. This result further validates the reliability of the molecular dynamics simulation findings.

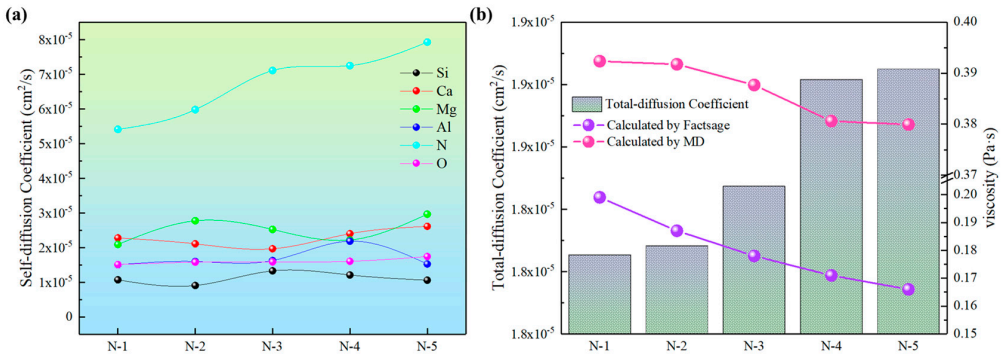


Figure 6. The fluidity variation in molten slag with different concentrations. (**a**) The variation in the self-diffusion coefficient of different ions. (**b**) The evolution of the total-diffusion coefficient and viscosity.

4. Conclusions

This research employs molecular dynamics simulations to elucidate the distinct regulatory effects of Na_2O and MgO on the structure and properties of aluminosilicate slags. The main findings are summarized as follows:

(1) The bond lengths of Si-O and Al-O remain essentially constant at approximately 1.61 Å and 1.73 Å, respectively, across varying Na_2O/MgO ratios. However, the Al-O coordination number decreases gradually from 4.45 to 4.32 with decreasing Na_2O content, indicating a structural transition of Al from fivefold (Al^5) to fourfold (Al^4) coordination.

(2) MgO promotes significant network depolymerization by transforming bridging oxygens and tricluster oxygens into non-bridging oxygens and free oxygens, exhibiting a stronger effect compared to Na_2O. Although Na_2O also disrupts BO and TO units, its contribution to network breakdown is relatively limited. The evolution of oxygen species is identified as the primary factor governing changes in network complexity.

(3) Despite the higher self-diffusion coefficient of Na^+ compared to Mg^{2+}, MgO more effectively enhances slag fluidity and reduces viscosity by decreasing the population of BO and TO while increasing NBO and FO. Both MD simulations and thermodynamic calculations show a consistent trend: the total diffusion coefficient increases and viscosity decreases with rising MgO content. In contrast, Na_2O requires a significantly higher concentration to achieve comparable effects on the melt dynamics.

Author Contributions: Conceptualization, C.J.; methodology, C.J.; software, C.J.; validation, C.J. and B.L.; formal analysis, C.J. and B.L.; investigation, C.J. and B.L.; writing—original draft preparation, C.J.; writing—review and editing, J.Z. and K.L.; supervision, J.Z. and K.L.; project administration, J.Z. and K.L.; funding acquisition, C.J. All authors have read and agreed to the published version of the manuscript.

Funding: This research was funded by the National Natural Science Foundation of China with grant number 52404336, China Postdoctoral Science Foundation with grant number 2024M750176 and Postdoctoral Fellowship Program of CPSF with grant number GZC20240109.

Data Availability Statement: The original contributions presented in this study are included in the article. Further inquiries can be directed to the corresponding authors.

Conflicts of Interest: The authors declare no conflicts of interest.

References

1. Yan, Z.-m.; Lv, X.-w.; Li, Z.-s. Physicochemical properties and structure of titania-containing metallurgical slags: A review. *J. Iron Steel Res. Int.* **2022**, *29*, 187–206. [CrossRef]
2. Yasipourtehrani, S.; Strezov, V.; Bliznyukov, S.; Evans, T. Investigation of thermal properties of blast furnace slag to improve process energy efficiency. *J. Clean. Prod.* **2017**, *149*, 137–145. [CrossRef]
3. Shi, C. Steel slag—Its production, processing, characteristics, and cementitious properties. *J. Mater. Civ. Eng.* **2004**, *16*, 230–236. [CrossRef]
4. Mills, K.; Yuan, L.; Li, Z.; Zhang, G.; Chou, K. A review of the factors affecting the thermophysical properties of silicate slags. *High Temp. Mater. Process.* **2012**, *31*, 301–321. [CrossRef]
5. Jiang, C.; Li, K.; Zhang, J.; Qin, Q.; Liu, Z.; Sun, M.; Wang, Z.; Liang, W. Effect of MgO/Al2O3 ratio on the structure and properties of blast furnace slags: A molecular dynamics simulation. *J. Non-Cryst. Solids* **2018**, *502*, 76–82. [CrossRef]
6. Zhou, C.; Li, J.; Wang, S.; Zhao, J.; Ai, L.; Chen, Q.; Chen, Q.; Zhao, D. Development of molecular dynamics and research progress in the study of slag. *Materials* **2023**, *16*, 5373. [CrossRef]
7. Liu, J.; Kong, W.; Yang, X.; Wang, Q.; He, Z.; Hou, X. Polymeric Structure Evolution Behavior Analysis of Aluminosilicate-Based Smelting Slag. *Metals* **2022**, *12*, 715. [CrossRef]
8. Kim, T.S.; Park, J.H. Structure-viscosity relationship of low-silica calcium aluminosilicate melts. *ISIJ Int.* **2014**, *54*, 2031–2038. [CrossRef]

9. Jiang, C.; Li, K.; Zhang, J.; Liu, Z.; Niu, L.; Liang, W.; Sun, M.; Ma, H.; Wang, Z. The effect of CaO and MgO on the structure and properties of coal ash in the blast furnace: A molecular dynamics simulation and thermodynamic calculation. *Chem. Eng. Sci.* **2019**, *210*, 115226. [CrossRef]
10. Ji, X.; Wang, Z.; Wang, X.; Zhao, X.; Zhang, H.; Zhang, T. Microstructures and properties of alkali-activated slags with composite activator: Effects of Na_2O equivalents. *J. Clean. Prod.* **2024**, *450*, 141754. [CrossRef]
11. Jiang, C.; Zhang, H.; Xiong, Z.; Chen, S.; Li, K.; Zhang, J.; Liang, W.; Sun, M.; Wang, Z.; Wang, L. Molecular dynamics investigations on the effect of Na_2O on the structure and properties of blast furnace slag under different basicity conditions. *J. Mol. Liq.* **2020**, *299*, 112195. [CrossRef]
12. Yu, K.; Zhang, Y.l.; Zhang, S.; Gao, M.; Zhou, C.Q. Effect of $Al_2O_3/TiO_2/Na_2O$ component in steelmaking slag on the corrosion of MgO refractories. *Ironmak. Steelmak.* **2023**, *50*, 648–657. [CrossRef]
13. El-Geassy, A.; Shehata, K.; Nasr, M.; Fakhoury, S. Effect of alkalies on the performance of blast furnace. *Trans. Iron Steel Inst. Jpn.* **1986**, *26*, 865–874. [CrossRef]
14. Shiau, J.-S.; Liu, S.-H.; Ho, C.-K. Effect of magnesium and aluminum oxides on fluidity of final blast furnace slag and its application. *Mater. Trans.* **2012**, *53*, 1449–1455. [CrossRef]
15. Vo, D.-H.; Hwang, C.-L.; Yehualaw, M.D.; Liao, M.-C. The influence of MgO addition on the performance of alkali-activated materials with slag−rice husk ash blending. *J. Build. Eng.* **2021**, *33*, 101605. [CrossRef]
16. Jiang, C.; Li, K.; Zhang, J.; Qin, Q.; Liu, Z.; Liang, W.; Sun, M.; Wang, Z. Molecular dynamics simulation on the effect of MgO/Al_2O_3 ratio on structure and properties of blast furnace slag under different basicity conditions. *Metall. Mater. Trans. B* **2019**, *50*, 367–375. [CrossRef]
17. Zhao, H.; Li, J.; Yang, S.; Liu, J.; Liu, W. Molecular dynamics study of structural properties of refining slag with various CaO/Al_2O_3 ratios. *Minerals* **2021**, *11*, 398. [CrossRef]
18. Plimpton, S. Fast parallel algorithms for short-range molecular dynamics. *J. Comput. Phys.* **1995**, *117*, 1–19. [CrossRef]
19. Evans, D.J.; Holian, B.L. The nose-hoover thermostat. *J. Chem. Phys.* **1985**, *83*, 4069–4074. [CrossRef]
20. Le Roux, S.; Petkov, V. ISAACS–interactive structure analysis of amorphous and crystalline systems. *Appl. Crystallogr.* **2010**, *43*, 181–185. [CrossRef]
21. Miyake, A. Interatomic potential parameters for molecular dynamics simulation of crystals in the system K_2O–Na_2O–CaO–MgO–Al_2O_3–SiO_2. *Mineral. J.* **1998**, *20*, 189–194. [CrossRef]
22. Bale, C.W.; Belisle, E.; Chartrand, P.; Decterov, S.A.; Eriksson, G.; Gheribi, A.E.; Hack, K.; Jung, I.-H.; Kang, Y.-B.; Melançon, J.; et al. Reprint of: FactSage thermochemical software and databases, 2010–2016. *Calphad* **2016**, *55*, 1–19. [CrossRef]
23. Lee, S.; Jung, B.; Lee, N.; Nam, W.; Lee, S.-J.; Yun, Y. Application of FactSage® thermodynamic modeling for predicting the ash transformation with temperatures under partial slagging entrained flow coal gasification condition. *Mater. Test.* **2018**, *60*, 163–172. [CrossRef]
24. van Dyk, J.C.; Waanders, F.B.; Benson, S.A.; Laumb, M.L.; Hack, K. Viscosity predictions of the slag composition of gasified coal, utilizing FactSage equilibrium modelling. *Fuel* **2009**, *88*, 67–74. [CrossRef]
25. Sun, Y.; Tan, M.; Li, T.; Li, J.; Shang, B. Study on the structural properties of refining slags by molecular dynamics with deep learning potential. *J. Mol. Liq.* **2022**, *353*, 118787. [CrossRef]
26. Michalet, X. Mean square displacement analysis of single-particle trajectories with localization error: Brownian motion in an isotropic medium. *Phys. Rev. E—Stat. Nonlinear Soft Matter Phys.* **2010**, *82*, 041914. [CrossRef]
27. Wu, T.; Wang, Q.; Yu, C.; He, S. Structural and viscosity properties of CaO-SiO_2-Al_2O_3-FeO slags based on molecular dynamic simulation. *J. Non-Cryst. Solids* **2016**, *450*, 23–31. [CrossRef]

Disclaimer/Publisher's Note: The statements, opinions and data contained in all publications are solely those of the individual author(s) and contributor(s) and not of MDPI and/or the editor(s). MDPI and/or the editor(s) disclaim responsibility for any injury to people or property resulting from any ideas, methods, instructions or products referred to in the content.